

ShieldNN: A Provably Safe NN Filter for Unsafe NN Controllers

James Ferlez^{*†}, Mahmoud Elnaggar^{**†}, Yasser Shoukry^{*}, and Cody Fleming^{***}

^{*}Electrical Engineering and Computer Science, University of California, Irvine

^{**}Electrical and Computer Engineering, University of Virginia

^{***}Mechanical Engineering, Iowa State University

Abstract—In this paper, we develop a novel closed-form Control Barrier Function (CBF) and associated controller shield for the Kinematic Bicycle Model (KBM) with respect to obstacle avoidance. The proposed CBF and shield — designed by an algorithm we call ShieldNN — provide two crucial advantages over existing methodologies. First, ShieldNN considers steering and velocity constraints directly with the non-affine KBM dynamics; this is in contrast to more general methods, which typically consider only affine dynamics and do not guarantee invariance properties under control constraints. Second, ShieldNN provides a closed-form set of safe controls for each state unlike more general methods, which typically rely on optimization algorithms to generate a single instantaneous control for each state. Together, these advantages make ShieldNN uniquely suited as an efficient Multi-Obstacle Safe Actions (i.e. multiple-barrier-function shielding) during training time of a Reinforcement Learning (RL) enabled Neural Network controller. We show via experiments that ShieldNN dramatically increases the completion rate of RL training episodes in the presence of multiple obstacles, thus establishing the value of ShieldNN in training RL-based controllers.

I. INTRODUCTION

Control Barrier Functions (CBF) [1] and the associated idea of controller shielding [2], [3], [4], [5], [6] have become important tools in the design of safety-critical control systems, especially those that incorporate learning-enabled components such as Neural Networks (NNs). However most of these techniques both assume affine dynamics (including with assumptions on relative degree) and use optimization problems to create shielding control actions, especially under control-input constraints. As a result, these methods add the computational cost of an additional optimization problem at each time step in order to apply their controller shields; this computational cost is particularly relevant when training a Reinforcement Learning (RL) based controller, whose training episodes ideally run much faster than real time. Moreover, incorporating an optimization problem into the shielding operation makes it difficult to reason about the availability of a safe control action in the multi-CBF case [7], [8].

In this paper, we propose the ShieldNN algorithm, which mitigates these downsides in the application-specific case of obstacle avoidance for the Kinematic Bicycle Model (KBM) (the KBM in turn being a good approximation for four-wheeled vehicles [9]). In particular, the ShieldNN algorithm can produce a closed-form, verified CBF with an associated optimization-free NN-based controller shield. Indeed, from the ShieldNN-designed CBF, it is effectively possible to obtain a set of safe controls for any particular state of the KBM dynamics. Thus, a ShieldNN-designed shield has two significant advantages. First, it is an ideal controller shield for

RL-based controller training, since it does not incur the cost of an optimization problem at each time step. Second, it can be easily extended from one obstacle (one CBF) to multiple obstacles case (multiple CBFs, one for each obstacle), since it effectively outputs closed form sets of safe controls; if the intersection of these sets is non-empty, then it provides a safe control for all of the obstacles simultaneously.

The main theoretical contribution of this paper is the ShieldNN algorithm, which is in turn based on a novel parameterized class of CBFs for the KBM dynamics and obstacle avoidance (see Section IV). Thus, ShieldNN takes as its input a particular instance of the KBM dynamics; a desired safety radius around an obstacle to be avoided; and a user-specified hyperparameter $\sigma \in [0, 1]$, which adjusts the “aggressiveness” of the resulting CBF and shield. ShieldNN then produces a CBF and controller shield using the following two components:

ShieldNN Verifier (Section V): This component verifies that the user-supplied KBM and safety radius are compatible with the chosen hyperparameter to indeed create a CBF. In the process, this component also verifies useful design properties of the set of safe controls admitted by the barrier function. *These properties admit an effective characterization of a guaranteed-safe set of controls.*

ShieldNN Synthesizer (Section VI): The result of the verification component is a barrier function where a crucial boundary between safe and non-safe controls is known to be convex in a particular state (of the KBM). *Thus, it is possible to soundly (and tightly) approximate the set of safe controls as function of KBM state, and to do so using a ReLU NN that approximates this boundary.* A further clipping operation yields a controller shield that provably restricts the control inputs to the set of safe controls specified by the CBF.

We further extend ShieldNN from the case of creating safe control actions to avoid a single obstacle to creating safe control actions to avoid multiple obstacles simultaneously. This extension appears in Section VII, and it follows from running multiple instances of the ShieldNN controller shield simultaneously: i.e. one instance per obstacle using the relative state for each obstacle. A safe actions can then be obtained by using an action that is safe for all controller shield instances (and treating the absence of such actions as a run-time diagnostic of un-safety). We validate the performance of this controller shield via experiments detailed in Section VIII.

Related Work. For an extensive and recent survey of the field of “safety shields (or filters),” we refer the reader to [10], [3]. Compared to the techniques reported in [10], [3], our proposed algorithms provide several critical advantages.

[†] Equally contributing first authors

This work was partially sponsored by the NSF awards #CNS-2002405, #CNS-2013824 and #CPS-1739333.

In particular, and unlike other techniques, ShieldNN aims to find closed-form characterization of the set of safe control actions. This set of safe control actions can then be directly mapped into neural network layers, hence bypassing the need to solve an optimization problem, which affects the real-time execution of the control pipeline. Moreover, the obtained characterization of the safe set of control inputs leads to a natural extension of handling multiple obstacles at once, which is an issue for several of the techniques reported in [10], [3].

II. PRELIMINARIES

A. Notation

Let \mathbb{R} denote the real numbers, and let $\|\cdot\|$ denote the Euclidean norm on \mathbb{R}^n . A (K -layer) ReLU network, is a function $\mathcal{N} = (L_{\theta(K)} \circ L_{\theta(K-1)} \circ \dots \circ L_{\theta(1)})(x)$ where $L_{\theta} : \mathbb{R}^i \rightarrow \mathbb{R}^o$ with $z \mapsto \max\{Wz + b, 0\}$, and the max is taken element-wise and $\theta^{(k)} = (W_k, b_k)$. $L_{\theta(K)}$ lacks the max operation by convention.

B. Control Barrier Functions

We introduce the following corollary, Corollary 1, which serves as the foundation of controller shielding [11].

Corollary 1. *Let $h : \mathbb{R}^n \rightarrow \mathbb{R}$ with $C_h \triangleq \{x \in \mathbb{R}^n | h(x) \geq 0\}$, and let $\mathcal{D} \subseteq \mathbb{R}^n$ s.t. $C_h \subseteq \mathcal{D}$. Further let $\dot{x} = f(x, u)$ be a control system where $f : \mathbb{R}^n \times \Omega_{\text{admis.}} \rightarrow \mathbb{R}^n$ is Lipschitz continuous. Finally, let α be a class \mathcal{K} function. If the set*

$$R_{h,\alpha}(x) \triangleq \{u \in \Omega_{\text{admis.}} | \nabla_x^T h(x) f(x, u) + \alpha(h(x)) \geq 0\} \quad (1)$$

is non-empty for each $x \in \mathcal{D}$, and a Lipschitz-continuous feedback controller $\mu : x \mapsto u$ satisfies

$$\mu(x) \in R_{h,\alpha}(x) \quad \forall x \in \mathcal{D} \quad (2)$$

then C_h is forward invariant for dynamics $f(\cdot, \mu(\cdot))$.

Proof. This follows directly from an application of zeroing barrier functions [12, Theorem 3]. \square

III. PROBLEM FORMULATION

We consider the kinematic bicycle model (KBM) as our dynamical system model, however, we consider the KBM described in terms of vehicle-to-obstacle relative position variables (e.g. measurable via LiDAR). That is, the distance to the obstacle, $\|\bar{r}\|$, and the angle of the vehicle with respect to the obstacle, ξ , are states in the dynamical system:

$$\begin{pmatrix} \dot{r} \\ \dot{\xi} \\ \dot{v} \end{pmatrix} = f_{\text{KBM}} \left(\begin{pmatrix} r \\ \xi \\ v \end{pmatrix}, \begin{pmatrix} a \\ \beta \end{pmatrix} \right) \triangleq \begin{pmatrix} v \cos(\xi - \beta) \\ -\frac{1}{r} v \sin(\xi - \beta) - \frac{v}{\ell_r} \sin(\beta) \\ a \end{pmatrix} \quad (3)$$

$$\beta \triangleq \tan^{-1} \left(\frac{\ell_r}{\ell_f + \ell_r} \tan(\delta_f) \right); \quad \chi \triangleq \begin{pmatrix} r \\ \xi \\ v \end{pmatrix}; \quad \omega \triangleq \begin{pmatrix} a \\ \beta \end{pmatrix}$$

where $r(t) \triangleq \|\bar{r}(t)\|$; a is the linear acceleration input; δ_f is the front-wheel steering angle input¹; and ξ is the angle of the vehicle to the obstacle. For clarity, we note a few special cases: when $\xi = \pm\pi/2$, the vehicle is oriented tangentially to the obstacle, and when $\xi = \pi$ or 0 , the vehicle is pointing directly at or away from the obstacle, respectively (see Fig. 1). β is an intermediate quantity, an *invertible function* of δ_f .

¹That is the steering angle can be set instantaneously, and the dynamics of the steering rack can be ignored.

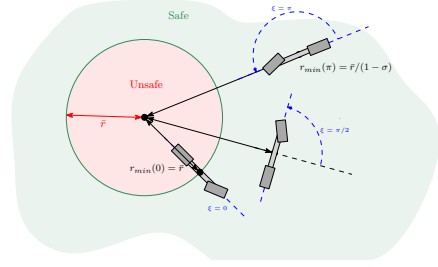


Fig. 1: Obstacle specification and minimum barrier distance as a function of relative vehicle orientation, ξ .

We make the further assumption that the KBM has a control constraint on δ_f such that $\delta_f \in [-\delta_{f,\max}, \delta_{f,\max}]$. To simplify further notation, we will consider β directly as a control variable; this is without loss of generality, since there is a bijection between β and the actual steering control angle, δ_f . Thus, β is also constrained: $\beta \in [-\beta_{\max}, \beta_{\max}]$, so the control vector is constrained $\omega \in \Omega_{\text{admis.}} \triangleq \mathbb{R} \times [-\beta_{\max}, \beta_{\max}]$.

Problem 1. *Consider a KBM vehicle with maximum steering angle $\delta_{f,\max}$, length parameters $\ell_f = \ell_r$ and maximum velocity v_{\max} . Consider also a disk-shaped region of radius \bar{r} centered at the origin, $U = \{x \in \mathbb{R}^2 : \|x\| \leq \bar{r}\}$. Find a set of safe initial conditions, S_0 , and a ReLU NN:*

$$\mathcal{N} : (\chi, \omega) \mapsto \hat{\omega} \quad (4)$$

such that for any globally Lipschitz continuous controller $\mu : \chi \mapsto \omega \in \Omega_{\text{admis.}}$, the state feedback controller:

$$\mathcal{N}(\chi, \mu(\chi)) : \chi \mapsto \hat{\omega} \quad (5)$$

is guaranteed to prevent the vehicle from entering the unsafe region U if it was started from a state in S_0 .

We also consider the multi-obstacle extension of Problem 1.

Problem 2. *Consider a KBM vehicle as in Problem 1, but instead consider P obstacles located at points $o_1, \dots, o_P \in \mathbb{R}^2$ and associated unsafe disks $U_p = \{x \in \mathbb{R}^2 : \|x - o_p\| \leq \bar{r}\}$, $p = 1, \dots, P$. Find a ReLU NN $\mathcal{N} : (\chi, \omega) \mapsto \hat{\omega}$ and a safety monitoring function*

$$S : (\chi, \omega) \mapsto s \in \{0, 1\} \quad (6)$$

such that if $S(\chi, \omega) = 1$ along a trajectory of the KBM dynamics under state feedback controller $\mathcal{N}(\chi, \mu(\chi)) : \chi \mapsto \hat{\omega}$, then the vehicle will not enter the unsafe set $\cup_{p=1}^P U_p$.

Our approach to solving Problem 1 is based on Corollary 1, and analogous to other approaches to shielding [11]. Thus, ShieldNN solves Problem 1 according to the following steps, using notation from Corollary 1 but dynamics (3):

(1) Design a Candidate Barrier Function (Section IV).

For a function, h , to be a barrier function for a specific safety property, its zero super-level set, C_h , must be contained in the set of safe states.

(2) Verify the Existence of Safe Controls (Section V).

(ShieldNN Verifier) Show that the set $R_{h,\alpha}(x)$ is non-empty for each state $x \in C_h$. This establishes that a safe feedback controller may exist.

²In our KBM model, this technically requires a feedback controller on a , but this won't affect our results.

(3) Design a Safety Filter (Section VI). (*ShieldNN Synthesizer*) If possible, design \mathcal{N}_0 such that $\mathcal{N}_0 : x \in \mathcal{C}_h \mapsto \hat{u} \in R_{h,\alpha}(x)$; then obtain a safety filter as:

$$\mathcal{N}(x, u) := \begin{cases} u & \text{if } u \in R_{h,\alpha}(x) \\ \mathcal{N}_0(x) & \text{if } u \notin R_{h,\alpha}(x). \end{cases} \quad (7)$$

Our approach to solving Problem 2 (see Section VII) is based on the availability of an estimate for the region $R_{h,\alpha}(x)$, as obtained from the ShieldNN CBF and controller shield (see above). In particular, we consider a ShieldNN-designed controller shield for each of the P obstacles individually (after shifting the KBM dynamics so that o_p is the origin), which provides a per-obstacle set of set of safe controls, $R_{h,\alpha}^{o_p}(x)$, $p = 1, \dots, P$. Testing whether the intersection $\cap_{p=1}^P R_{h,\alpha}^{o_p}(x)$ is nonempty yields the desired safety monitor S , and choosing a control from such a nonempty intersection yields a safety filter.

IV. BARRIER FUNCTION(S) FOR THE KBM DYNAMICS: THE BASIS OF SHIELDNN

We propose the following class of candidate barrier functions to certify control actions so that the vehicle doesn't get within \bar{r} units of the origin (Problem 1):

$$h_{\bar{r},\sigma}(\chi) = h_{\bar{r},\sigma}(\xi, r, v) = \frac{\sigma \cos(\xi/2) + 1 - \sigma}{\bar{r}} - \frac{1}{r} \quad (8)$$

where $\sigma \in (0, 1)$ is an additional parameter whose function we shall describe subsequently. First note that the equation $h_{\bar{r},\sigma}(\chi) = 0$ has a unique solution, $r_{\min}(\xi)$ for each of ξ :

$$r_{\min}(\xi) = \bar{r} / (\sigma \cos(\xi/2) + 1 - \sigma), \quad (9)$$

so the smallest value of r_{\min} is $r_{\min}(0) = \bar{r}$. Thus, the function $h_{\bar{r},\sigma}$ satisfies the requirements of (1) in the ShieldNN framework: i.e. $\mathcal{C}_{h_{\bar{r},\sigma}}$, the zero super-level set of $h_{\bar{r},\sigma}$, is entirely contained in the set of safe states as proscribed by Problem 1, independent of the choice of σ . See Fig. 1, which also depicts another crucial value, $r_{\min}(\pm\pi) = \bar{r}/(1 - \sigma)$.

Remark 1. Note that $h_{\bar{r},\sigma}$ is independent of the velocity state, v . This will ultimately force ShieldNN filters to intervene only by altering the steering input.

A barrier function also requires a class \mathcal{K} function, α . For ShieldNN, we choose a linear function

$$\alpha_{v_{\max}}(x) = K \cdot v_{\max} \cdot x \quad (10)$$

where v_{\max} is the assumed maximum velocity (Problem 1), and constant K is a selected according to the following.

Theorem 1. Consider any fixed \bar{r} , ℓ_r and σ . Assume that $0 \leq v \leq v_{\max}$ (as specified by Problem 1). If K is such that:

$$K \geq K_{\bar{r},\sigma} \triangleq \max(\{1, 1/\bar{r}\}) \cdot \left(\frac{\sigma}{2\bar{r}} + 2\right) \quad (11)$$

then the Lie derivative $\nabla_{\chi}^T h_{\bar{r},\sigma}(x) \cdot f_{\text{KBM}}(\chi, \omega) + \alpha(h_{\bar{r},\sigma}(\chi))$ is a monotonically increasing function in r for all $r \geq \bar{r}$ for

each fixed choice of $v \in (0, v_{\max}]$ and the remaining state and control variables.

In particular, for all $\chi \in \mathcal{C}_{h_{\bar{r},\sigma}}$ such that $v \in (0, v_{\max}]$ it is the case that:

$$R_{h_{\bar{r},\sigma}}((r_{\min}(\xi), \xi, v)) \subseteq R_{h_{\bar{r},\sigma}}(\chi). \quad (12)$$

where $R_{h_{\bar{r},\sigma}}$ has an analogous definition to that in Corollary 1 (but with the α subscript suppressed for brevity).

Proof. See Appendix II-B of [13]. \square

As a consequence of Theorem 1, define the following.

Definition 1. Define $\mathcal{L}_{\bar{r},\sigma,\ell_r}(\xi, \beta, v)$ according to Eq. (13).

In addition to concretely defining our class of candidate barrier functions, Theorem 1 is the essential facilitator of the ShieldNN algorithm. In particular, note that the right-hand side of (13) can be simplified as indicated, since $h_{\bar{r},\sigma}((r_{\min}(\xi), \xi, v)) = 0$ and $\alpha_{v_{\max}}(0) = 0$. Hence, the set $R_{h_{\bar{r},\sigma}}((r_{\min}(\xi), \xi, v))$ is independent of v , so (12) gives a sufficient condition for safe controls (2) in terms of a single state variable, ξ , and a single control variable β . This simplifies not only the ShieldNN verifier but also the ShieldNN synthesizer, as we demonstrate in the next section.

V. SHIELDNN VERIFIER

The overall ShieldNN algorithm has three inputs: the specs for a KBM vehicle ($\ell_f = \ell_r$, $\delta_{f,\max}$ and v_{\max}); the desired safety radius (\bar{r}); and the barrier parameter σ . Thus, the objective of the ShieldNN verifier is to soundly verify that these parameter values make equation (8) a true barrier function for Problem 1. From Theorem 1, it suffices to show that $R_{h_{\bar{r},\sigma}}((r_{\min}(\xi), \xi, \cdot)) \neq \emptyset$ for each $\xi \in [-\pi, \pi]$; the barrier property then follows by Corollary 1.

However, the ShieldNN verifier soundly verifies that each $R_{h_{\bar{r},\sigma}}((r_{\min}(\xi), \xi, \cdot))$ is nonempty by soundly verifying that these sets have certain structural properties. In particular, ShieldNN verifies that for each orientation angle, ξ , the set $R_{h_{\bar{r},\sigma}}((r_{\min}(\xi), \xi, \cdot))$ is an *interval* whose bounds are a continuous function of ξ and also clipped at the max/min steering inputs: i.e.

$$R_{h_{\bar{r},\sigma}}((r_{\min}(\xi), \xi, \cdot)) = [\max\{-\beta_{\max}, \mathbf{l}(\xi)\}, \min\{\beta_{\max}, \mathbf{u}(\xi)\}] \quad (14)$$

where \mathbf{l} and \mathbf{u} are continuous functions of ξ . Moreover, ShieldNN verifies that the function \mathbf{l} (resp. \mathbf{u}) is *concave* (resp. *convex*); indeed, the symmetry of the problem dictates that $\mathbf{u}(\xi) = -\mathbf{l}(-\xi)$. From these structural properties, it becomes straightforward to establish $R_{h_{\bar{r},\sigma}}((r_{\min}(\xi), \xi, \cdot)) \neq \emptyset$, and hence the desired conclusion as described above.

We reiterate that the ShieldNN verifier is only *sound*, and so may fail to verify the structural properties described above. However, this has not been observed in practice. See Fig. 2a for an illustrative example with parameters $\ell_f = \ell_r = 2$ m, $\bar{r} = 4$ m, $\beta_{\max} = 0.4636$ and $\sigma = 0.48$; $\cup_{\xi \in [-\pi, \pi]} R_{h_{\bar{r},\sigma}}((r_{\min}(\xi), \xi, \cdot))$ is shown in light green, and \mathbf{l} and \mathbf{u} are shown in dark green.

$$\begin{aligned} \mathcal{L}_{\bar{r},\sigma,\ell_r}(\xi, \beta, v) &\triangleq \left[\nabla_{\chi}^T h_{\bar{r},\sigma}(\chi) \cdot f_{\text{KBM}}(\chi, \omega) + \alpha(h_{\bar{r},\sigma}(\chi)) \right]_{\chi=(r_{\min}(\xi), \xi, v)} \\ &= v \left(\frac{\sigma}{2\bar{r} \cdot r_{\min}(\xi)} \sin\left(\frac{\xi}{2}\right) \sin(\xi - \beta) + \frac{\sigma}{2\bar{r} \cdot \ell_r} \sin\left(\frac{\xi}{2}\right) \sin(\beta) + \frac{1}{r_{\min}(\xi)^2} \cos(\xi - \beta) \right) \end{aligned} \quad (13)$$

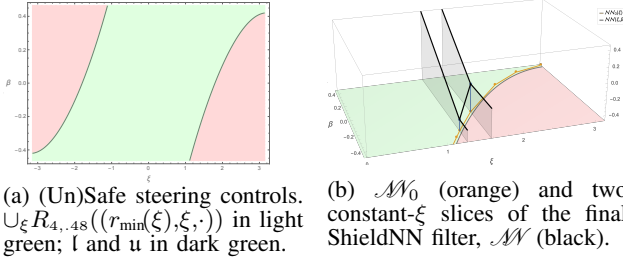


Fig. 2: Illustrated ShieldNN products for $\ell_f = \ell_r = 2$ m, $\bar{r} = 4$ m, $\beta_{\max} = 0.4636$, $\sigma = 0.48$.

A. Algorithmic Verification of (14)

Recall that the main function of the ShieldNN verifier is to soundly verify that equation (14) holds for a concave function l and with $u(\xi) = -l(-\xi)$. The conclusion about u follows directly from the symmetry of the problem, so we focus on the claims for l .

We now make the following observation.

Proposition 1. *Suppose that (14) holds with $u(\xi) = -l(-\xi)$, and let $\mathcal{L}_{\bar{r}, \sigma, \ell_r}$ be as in Definition 1. Then for any $\xi' \in [-\pi, \pi]$ such that $l(\xi') \in (-\beta_{\max}, \beta_{\max})$ it is the case that*

$$\mathcal{L}_{\bar{r}, \sigma, \ell_r}(\xi', l(\xi'), \cdot) = 0. \quad (15)$$

Proof. This follows from the definition of $R_{h_{\bar{r}, \sigma}}$, and the fact that we are evaluating it on the barrier, i.e. for $\chi' = (r_{\min}(\xi'), \xi', v)$. Thus, $h(\chi') = 0$, and $\alpha_{v_{\max}}(h(\chi')) = 0$. \square

This suggests that (15) can be used to establish the claim in (14). Thus, let $a < b$ be real numbers, and define:

$$\text{bd}_{[a, b]} \triangleq \{(\xi', \beta') \in [a, b] \times [-\beta_{\max}, \beta_{\max}] \mid \mathcal{L}_{\bar{r}, \sigma, \ell_r}(\xi', \beta', \cdot) = 0\} \quad (16)$$

with the appropriate modifications for other interval types (a, b) , $(a, b]$ and $[a, b)$. We also define a related quantity:

$$\text{dom}(\text{bd}_{[a, b]}) = \{\xi \in [a, b] \mid \exists \beta. (\xi, \beta) \in \text{bd}_{[a, b]}\}. \quad (17)$$

We thus develop a sound algorithm to verify (14) and the concavity of l by soundly verifying these properties in order:

Property 1. Show that $\text{bd}_{[-\pi, \pi]} \cap ([-\pi, \pi] \times \{-\beta_{\max}\}) = \{(\xi_0, \beta_{\max})\}$; that is $\text{bd}_{[-\pi, \pi]}$ intersects the lower control constraint a single orientation angle, ξ_0 . Likewise $\text{bd}_{[-\pi, \pi]} \cap ([-\pi, \pi] \times \beta_{\max}) = \{(-\xi_0, \beta_{\max})\}$ by symmetry.

Property 2. Verify that $\text{bd}_{[\xi_0, \pi]}$ is the graph of a function (likewise for $\text{bd}_{[-\pi, -\xi_0]}$ by symmetry), and $\text{bd}_{(-\xi_0, \xi_0)} = \emptyset$. Thus, define l as $\text{graph}(l) \triangleq \text{bd}_{[\xi_0, \pi]}$.

Property 3. Verify that l in **Property 2** is concave.

The ShieldNN verifier expresses each of these properties as the sound verification that a particular function is greater than zero on a subset of its domain. The functions that are associated with these properties are either $\mathcal{L}_{\bar{r}, \sigma, \ell_r}$ itself or else derived from it (i.e. by differentiating), so each is an analytic function where ξ and β appear only in trigonometric functions. These surrogate verification problems are amenable to over-approximation and the Mean-Value Theorem.

With this program in mind, Section V-B - Section V-D explain how to express **Property 1-3** as minimum-verification problems. Section V-E describes main algorithmic component of the ShieldNN verifier, *CertifyMin*.

B. Verifying Property 1

To verify **Property 1**, we can start by using a numerical root finding algorithm to find a zero of $\mathcal{L}_{\bar{r}, \sigma, \ell_r}(\xi, -\beta_{\max}, \cdot)$, viewed as a function of ξ (Definition 1). However, there is no guarantee that this root, call it $\hat{\xi}_0$ is the only root on the set $[-\pi, \pi] \times \{-\beta_{\max}\}$. In this case, the property to be verified reduces to the following.

Proposition 2. *Suppose that $\mathcal{L}_{\bar{r}, \sigma, \ell_r}(\hat{\xi}_0, -\beta_{\max}, \cdot) = 0$ (Definition 1). Also, suppose that there exists an $\epsilon > 0$ such that:*

- 1) $\forall \xi \in [-\pi, \hat{\xi}_0 - \epsilon] \cdot \mathcal{L}_{\bar{r}, \sigma, \ell_r}(\hat{\xi}_0 - \epsilon, -\beta_{\max}, \cdot) > 0$;
- 2) $\mathcal{L}_{\bar{r}, \sigma, \ell_r}(\hat{\xi}_0 - \epsilon, -\beta_{\max}, \cdot) > 0$ and $\mathcal{L}_{\bar{r}, \sigma, \ell_r}(\pi, -\beta_{\max}, \cdot) < 0$;
- 3) $\forall \xi \in [\hat{\xi}_0 - \epsilon, \pi] \cdot \frac{\partial^2}{\partial \xi^2} \mathcal{L}_{\bar{r}, \sigma, \ell_r}(\xi, -\beta_{\max}, \cdot) > 0$.

*Then $\hat{\xi}_0$ is the only root of $\mathcal{L}(\xi, -\beta_{\max}, \cdot)$ on $[-\pi, \pi] \times \{-\beta_{\max}\}$. That is **Property 1** is verified.*

Proof. If (i) is true, then no zeros of $\mathcal{L}_{\bar{r}, \sigma, \ell_r}$ lie in $[-\pi, \hat{\xi}_0 - \epsilon]$.

If (iii) is true, then $\mathcal{L}_{\bar{r}, \sigma, \ell_r}(\xi, -\beta_{\max}, \cdot)$ is a convex function of ξ on the interval $[\hat{\xi}_0, \pi]$. But if (ii) is also true, then $\hat{\xi}_0$ must be the only zero of $\mathcal{L}_{\bar{r}, \sigma, \ell_r}$ on the same interval. This follows by contradiction from the assertion of convexity. If there were another zero on $(\hat{\xi}_0, \pi]$, then the line connecting $(\hat{\xi}_0, \mathcal{L}_{\bar{r}, \sigma, \ell_r}(\hat{\xi}_0, -\beta_{\max}, \cdot))$ and $(\pi, \mathcal{L}_{\bar{r}, \sigma, \ell_r}(\pi, -\beta_{\max}, \cdot))$ would lie below this point by assumption (ii), hence contradicting convexity. A similar argument can be made if there were a zero on $[\hat{\xi}_0 - \epsilon, \hat{\xi}_0)$. \square

Crucially, the conditions (i)-(iii) of Proposition 2 are conditions that can be checked either by verifying that a function is greater than 0 on an interval (as for (ii) and (iii)), or else $\mathcal{L}_{\bar{r}, \sigma, \ell_r}$ has a particular sign for particular inputs (as in (i)). Thus, ShieldNN verifier can establish **Property 1** by means of the *CertifyMin* function that we propose later.

C. Verifying Property 2

Our verification of **Property 2** depends on the conclusion of **Property 1**. In particular, let $\xi_0 = \hat{\xi}_0$ be the single root of $\mathcal{L}_{\bar{r}, \sigma, \ell_r}$ on $([-\pi, \pi] \times \{-\beta_{\max}\})$ as verified above. As before, the proposition below gives sufficient conditions to assert **Property 2**, and where verifying those conditions requires at worst checking the sign of some $\mathcal{L}_{\bar{r}, \sigma, \ell_r}$ -derived function on an interval (or rectangle).

The main technique for proving that $\text{bd}_{[\xi_0, \pi]}$ is the graph of a function is to note that constant-level curves of $\mathcal{L}_{\bar{r}, \sigma, \ell_r}$ are solutions to the ODE defined by its gradient. In particular, then, $\text{bd}_{[\xi_0, \pi]}$ contains such a solutions in the rectangle of interest, since it is a subset of the zero-constant level curve of $\mathcal{L}_{\bar{r}, \sigma, \ell_r}$. Thus, we can verify the desired properties of $\text{bd}_{[\xi_0, \pi]}$ by considering the aforementioned ODE, and demonstrating that it has only one solution in the rectangle of interest.

Proposition 3. *Let ξ_0 be as above. Now suppose the following two conditions are satisfied:*

- 1) $\frac{\partial}{\partial \xi} \mathcal{L}_{\bar{r}, \sigma, \ell_r}(\xi_0, -\beta_{\max}, \cdot) > 0$;
- 2) for all $(\xi, \beta) \in ([\xi_0, \pi] \times [-\beta_{\max}, \beta_{\max}])$ it is true that

$$\frac{\partial}{\partial \beta} \mathcal{L}_{\bar{r}, \sigma, \ell_r}(\xi, \beta, \cdot) < 0; \text{ and} \quad (18)$$

- 3) there exists $\epsilon > 0$ and $\hat{\beta}_0 \in [-\beta_{\max}, \beta_{\max}]$ such that
 - a) $\forall \xi \in [-\beta_{\max}, \hat{\beta}_0 - \epsilon] \cdot \mathcal{L}_{\bar{r}, \sigma, \ell_r}(\pi, \hat{\beta}_0 - \epsilon, \cdot) < 0$;
 - b) $\forall \beta \in [\hat{\beta}_0 - \epsilon, \beta_{\max}] \cdot \frac{\partial}{\partial \beta} \mathcal{L}_{\bar{r}, \sigma, \ell_r}(\pi, \beta, \cdot) > 0$.

Then $\text{bd}_{[\xi_0, \pi]}$ is the graph of a function, and we can define the function \mathbf{l} on $[\xi_0, \pi]$ by $\text{graph}(\mathbf{l}) \triangleq \text{bd}_{[\xi_0, \pi]}$.

Proof. Consider the two-state ODE defined by:

$$\dot{\xi} = -\frac{\partial}{\partial \beta} \mathcal{L}_{\bar{r}, \sigma, \ell_r}(\xi, \beta, \cdot); \quad \dot{\beta} = \frac{\partial}{\partial \xi} \mathcal{L}_{\bar{r}, \sigma, \ell_r}(\xi, \beta, \cdot). \quad (19)$$

The solutions to (19) are guaranteed to exist and be unique on $[\xi_0, \pi] \times [-\beta_{\max}, \beta_{\max}]$, since the vector field is locally Lipschitz on that rectangle (it is differentiable). Thus, any solution of (19) is guaranteed to follow a constant-level curve of $\mathcal{L}_{\bar{r}, \sigma, \ell_r}$ within this rectangle; the particular constant-level curve matches the value of $\mathcal{L}_{\bar{r}, \sigma, \ell_r}$ for its initial condition.

As a first step, we establish two facts about the solution of (19) with initial condition $(\xi_0, -\beta_{\max})$:

- 1) the β component of this solution strictly increases; and
- 2) the solution exits $[\xi_0, \pi] \times [-\beta_{\max}, \beta_{\max}]$ only through its $\xi = \pi$ edge.

First note that some initial portion of this solution must be contained in $[\xi_0, \pi] \times [-\beta_{\max}, \beta_{\max}]$ by assumption (i) and assumption (ii) applied to $(\xi_0, -\beta_{\max})$. Statement 1 is thus established directly by assumption (ii). Now we establish 2). Note that the solution cannot exit via the $\xi = \xi_0$ edge because its β component is strictly increasing. And it can't exit the $\beta = \mp \beta_{\max}$ edges either, because we have verified that $\mathcal{L}_{\bar{r}, \sigma, \ell_r}$ has only one root on each edge, $(\xi, -\beta_{\max})$ and $(-\xi_0, \beta_{\max})$, respectively. This leaves only the $\xi = \pi$ edge. The solution must leave this rectangle eventually, by the exclusion of the other edges and the fact that its β component is strictly increasing. Thus, it exits via the $\xi = \pi$ edge.

The final conclusion about the functionality follows if $\text{bd}_{[\xi_0, \pi]}$ if $\text{bd}_{[\xi_0, \pi]}$ corresponds *exactly* to the single, unique solution described above. To verify this, we need to verify that there is a single root of $\mathcal{L}_{\bar{r}, \sigma, \ell_r}$ along the $\xi = \pi$ edge, much as we did to verify **Property 1**; this is made possible by assumption (iii), items (I)-(II). \square

As in the case of Proposition 2, the conditions of Proposition 3 are conditions that can be checked using the `CertifyMin` function that we will propose subsequently.

D. Verifying Property 3

We verify **Property 3** starting from the assumption that verifications of **Property 1** and **Property 2** were successful. In particular, we assume a function \mathbf{l} with domain $[\xi_0, \pi]$ that defines the lower boundary of the set $R_{h_{\bar{r}, \sigma}}$, and which is characterized entirely by $\mathcal{L}_{\bar{r}, \sigma, \ell_r}(\xi, \mathbf{l}(\xi), \cdot) = 0$.

Since \mathbf{l} corresponds exactly to such a constant-level contour, we can use derivatives of $\mathcal{L}_{\bar{r}, \sigma, \ell_r}$ to compute the derivative of \mathbf{l} with respect to ξ . That is if we define

$$\gamma'(\xi, \beta) \triangleq -\frac{\partial \mathcal{L}_{\bar{r}, \sigma, \ell_r} / \partial \xi}{\partial \mathcal{L}_{\bar{r}, \sigma, \ell_r} / \partial \beta}(\xi, \beta) \quad (20)$$

then $\mathbf{l}'(\xi) = \gamma'(\xi, \mathbf{l}(\xi))$.

By extension then, it is possible to derive the *second* derivative of \mathbf{l} using $\mathcal{L}_{\bar{r}, \sigma, \ell_r}$ if we define:

$$\gamma''(\xi, \beta) \triangleq \frac{\partial}{\partial \xi} \gamma'(\xi, \beta) + \frac{\partial}{\partial \beta} \gamma'(\xi, \beta) \cdot \gamma'(\xi, \beta) \quad (21)$$

so that $\mathbf{l}''(\xi) = \gamma''(\xi, \mathbf{l}(\xi))$. This gives us a sufficient condition for the *concavity* of \mathbf{l} .

Proposition 4. Suppose that ξ_0 and $\text{graph}(\mathbf{l}) \triangleq \text{bd}_{[\xi_0, \pi]}$ as above. If for all $(\xi, \beta) \in [\xi_0, \pi] \times [-\beta_{\max}, \beta_{\max}]$ we have that

$$\gamma''(\xi, \beta) < 0 \quad (22)$$

then \mathbf{l} is concave.

Proof. Direct from the calculations above. \square

E. CertifyMin and the ShieldNN Verifier

Together, **Properties 1-3** are sufficient to prove that a particular set of parameters leads $h_{\bar{r}, \sigma}$ to be a barrier function for the KBM. Furthermore, each of these conditions involves asserting that $\mathcal{L}_{\bar{r}, \sigma, \ell_r}$ or its derivatives are strictly positive or negative on an interval or a rectangle.

Since $\mathcal{L}_{\bar{r}, \sigma, \ell_r}$ is composed of simple functions, it is possible for a computer algebra system (CAS) to not only obtain each of these verification functions automatically, but to further differentiate each of them once *more*. Thus, we can combine an extra derivative with the Mean-Value Theorem to verify each of these individual claims. We describe this procedure as `CertifyMin` below.

Algorithm 1: `CertifyMin`.

```

input : function  $f(\xi, \beta)$  that is either  $\mathcal{L}_{\bar{r}, \sigma, \ell_r}$  or one of its
         derivatives;  $\xi$ -interval  $[\xi_\ell, \xi_h]$ ;  $\beta$ -interval  $[\beta_\ell, \beta_h]$ ; a sign
          $s = \pm 1$ . Either  $\xi_\ell = \xi_h$  or  $\beta_\ell = \beta_h$  but not both.
output: N_est

1 function CertifyMin( $f, \xi_\ell, \xi_h, \beta_\ell, \beta_h, s$ )
2    $\text{Df} \leftarrow \text{SymbolicGradient}(f)$ 
3   if  $\xi_\ell = \xi_h$  then
4      $\text{DfNorm} \leftarrow$ 
        $\text{SymbolicNorm}(\text{SymbolicGetComponent}(\text{Df}, \beta))$ 
5   else if  $\beta_\ell = \beta_h$  then
6      $\text{DfNorm} \leftarrow$ 
        $\text{SymbolicNorm}(\text{SymbolicGetComponent}(\text{Df}, \xi))$ 
7   else
8      $\text{DfNorm} \leftarrow \text{SymbolicNorm}(\text{Df})$ 
9   end
10   $\text{gridSize} \leftarrow 1$ 
11   $\text{refine} \leftarrow \text{True}$ 
12  while  $\text{refine}$  do
13     $\text{gridSize} \leftarrow \text{gridSize}/10$ 
14     $\text{refine} \leftarrow \text{False}$ 
15    for  $(\xi', \beta')$  in GridIterator( $\text{gridSize}, \xi_\ell, \xi_h, \beta_\ell, \beta_h$ ) do
16      if  $s \cdot f(\xi', \beta') < 0$  then
17        return False
18      else if  $s \cdot f(\xi', \beta') < \sqrt{2} \cdot \text{gridSize}$  then
19         $\text{DfNorm}(\xi', \beta') \text{ then}$ 
20         $\text{refine} \leftarrow \text{True}$ 
21        break
22    end
23  end
24  return True
25 end

```

VI. SHIELDNN SYNTHESIZER

Given a barrier function, recall from (3) in Section III that synthesizing a ShieldNN filter entails two components: \mathcal{N}_0 and \mathcal{N} . That is \mathcal{N}_0 chooses a *safe* control for each state, and \mathcal{N} overrides *unsafe* controls with the output of \mathcal{N}_0 .

Design of \mathcal{N}_0 . This task is much easier than it otherwise would be, since the ShieldNN verifier also verifies the safe controls as lying between the continuous functions $\max\{-\beta_{\max}, \mathbf{l}\}$ and $\min\{\beta_{\max}, \mathbf{u}\}$ where \mathbf{l} and \mathbf{u} are concave and $\mathbf{u}(\xi) = -\mathbf{l}(-\xi)$. In particular, then, it is enough to design \mathcal{N}_0 as any neural network such that

$$\max\{-\beta_{\max}, \mathbf{l}\} \leq \mathcal{N}_0 \leq \min\{\beta_{\max}, \mathbf{u}\}. \quad (23)$$

This property can be achieved in several ways, including training against samples of $\max\{-\beta_{\max}, \mathbf{l}\}$ for example.

However, we chose to synthesize \mathcal{N}_0 directly in terms of tangent line segments to l (and thus exploit the *concavity* of l). A portion of just such a function \mathcal{N}_0 is illustrated by the orange line in Fig. 2b.

Design of \mathcal{N} . Since the value of \mathcal{N}_0 is designed to lie inside the interval of safe controls, the function \mathcal{N}_0 can itself be used to decide when an unsafe control is supplied. In particular, using this property and the symmetry $u(\xi) = -l(-\xi)$, we can simply choose

$$\mathcal{N} : \beta \mapsto \min\{\max\{\mathcal{N}_0(\beta), \beta\}, -\mathcal{N}_0(-\beta)\}. \quad (24)$$

Note: the closer \mathcal{N}_0 approximates its lower bound, $\max\{-\beta_{\max}, l\}$, the less intrusive the safety filter. Two constant- ξ slices of such a \mathcal{N} are shown in Fig. 2b.

VII. EXTENDING SHIELDNN TO MULTIPLE OBSTACLES

We now consider the general case of multiple obstacles in the environment. We propose two approaches: 1) a Single-Obstacle Safe-Action (SOSA). 2) a Multi-Obstacle-Safe-Action (MOSA) approach which is described in Algorithm 2.

1) *SOSA*: We start by sorting the detected obstacle states during runtime according to their distances r from the vehicle. Then, we choose the closest obstacle and directly apply the synthesized ShieldNN \mathcal{N} to the controller steering action in order to generate safe steering control actions that are safe considering only the current closest obstacle.

2) *MOSA*: The goal is to search inside the state-action space for an action that is safe for all detected obstacles in the environment. Let $\Xi = \{\xi_1, \xi_2, \dots, \xi_N\}$ is the list of angles ξ for all detected obstacles sorted by the closest to the furthest obstacle to the vehicle. First, we get the lower and upper bounds of the safe action interval for each ξ_i as follows: i) if $\xi_i > 0$, then the corresponding safe action interval is $[-\beta_{\max}, \mathcal{N}_0(\xi)]$ otherwise, the safe action interval is $[-\beta_{\max}, -\mathcal{N}_0(-\xi)]$. This is due to the symmetry of the boundary between safe and unsafe regions as shown in Fig. 2a. Second, we find the common safe action interval between all detected obstacles by getting the intersection of these intervals. If the intersection is an empty interval, this means that we cannot find an action that is guaranteed to be safe for all detected obstacles. In that case, we fall back to SOSA, generate a safe action considering the closest obstacle $\mathcal{N}(\Xi[0])$ and raise a flag indicating that no safe action can be found. If the unsafe controller is a learning based controller (e.g. a neural network), the unsafe action flag is used to train the unsafe controller on avoiding moving the vehicle to a state where no common safe action for all detected obstacles can be found. When the intersection interval is nonempty, we use a safe control action β^* inside the intersection that is closest to the input unsafe action β .

VIII. SHIELDNN EVALUATION

We conduct a series of experiments to evaluate ShieldNN's performance when applied to unsafe RL controllers. The CARLA Simulator [14] is used as our RL environment, and we consider an RL agent whose goal is to drive a simulated vehicle while avoiding the obstacles in the environment. The goals of the experiments are to assess the following:

- 1) The safety of the RL agent when ShieldNN is applied after training (Experiment 1).
- 2) The robustness of ShieldNN when applied in a different environment than that used in training (Experiment 2).

Algorithm 2: MOSA.

input : Array Ξ contains the list of ξ angles for all detected obstacles sorted by the closest to furthest from the vehicle, $\beta, \beta_{\max}, \mathcal{N}_0, \mathcal{N}$

output: $\beta^*, \text{SafeAction}$

```

1 function MOSA( $\Xi, \beta, \beta_{\max}, \mathcal{N}_0, \mathcal{N}$ )
2   SafeIntervalsLBs, SafeIntervalsUBs  $\leftarrow$  new Array
3   foreach  $\xi \in \Xi$  do
4     if  $\xi \geq 0$  then
5       SafeIntervalsLBs.insert( $\mathcal{N}_0(\xi)$ )
6       SafeIntervalsUBs.insert( $\beta_{\max}$ )
7     else
8       SafeIntervalsLBs.insert( $-\beta_{\max}$ )
9       SafeIntervalsUBs.insert( $\mathcal{N}_0(\xi)$ )
10    end
11    IntersectionLB  $\leftarrow$  max(SafeIntervalsLBs)
12    IntersectionUB  $\leftarrow$  min(SafeIntervalsUBs)
13  end
14  if IntersectionUB  $\geq$  IntersectionLB then
15    SafeAction  $\leftarrow$  true
16    if  $\beta \in [\text{IntersectionLB}, \text{IntersectionUB}]$  then
17       $\beta^* \leftarrow \beta$ 
18    else if  $\beta > \text{IntersectionUB}$  then
19       $\beta^* \leftarrow \text{IntersectionUB}$ 
20    else
21       $\beta^* \leftarrow \text{IntersectionLB}$ 
22    end
23  else
24     $\beta^* \leftarrow \mathcal{N}(\Xi[0], \beta), \text{SafeAction} \leftarrow \text{false}$ 
25  end
26  return  $\beta^*, \text{SafeAction}$ 
27 end

```

- 3) The effect of applying SOSA and MOSA approaches on the RL agent in case of having an environment with multiple obstacles in terms of safety (Experiment 3).

RL Task: The RL task is to drive a simulated four-wheeled vehicle from point A to point B on a curved road that is populated with obstacles. The obstacles are static CARLA pedestrian actors randomly spawned at different locations between the two points. We define unsafe states as those in which the vehicle hits an obstacle. As ShieldNN is designed for obstacle avoidance, we do not consider the states when the vehicle hits the sides of the roads to be unsafe with respect to ShieldNN. Technical details and graphical representations are included in the Supplementary Materials.

Reward function and termination criteria: If the vehicle reaches point B, the episode terminates, and the RL agent gets a reward value of a 100. The episode terminates, and the agent gets penalized by a value of a 100 in the following cases: when the vehicle (i) hits an obstacle; (ii) hits one of the sides of the road; (iii) has a speed lower than 1 KPH after 5 seconds from the beginning of the episode; or (iv) has a speed that exceed the maximum speed (45 KPH). The reward function is a weighted sum of four terms, and the weights were tuned during training. The four terms are designed in order to incentivize the agent to keep the vehicle's speed between a minimum speed (35 KPH) and a target speed (40 KPH), maintain the desired trajectory, align the vehicle's heading with the direction of travel, and keep the vehicle away from obstacles.

Integrating ShieldNN with PPO: We train a Proximal Policy Optimization (PPO) [15] neural network in order to perform the desired RL task. To speed up policy learning as in [16], we encode the front camera feed into a latent vector using the encoder part of a trained β -Variational Auto-Encoder (β -VAE). The encoder takes 160x80 RGB images generated by the simulated vehicle's front facing camera

Config	Training		Testing	Experiment 2		Experiment 3A	
	Obstacle	Filter	Filter	TC% ¹	OHR% ²	TC% ¹	OHR% ²
1	OFF	OFF	OFF	7.59	99.5	27.53	79.5
2	OFF	OFF	ON	98.82	0.5	98.73	0.5
3	ON	OFF	OFF	94.82	8.5	71.88	34
4	ON	OFF	ON	100	0	100	0
5	ON	ON	OFF	62.43	44	50.03	60
6	ON	ON	ON	100	0	100	0

¹ TC% := Track Completion % ² OHR% := Obstacle Hit Rate %

TABLE I: Experiment 1 & 2, evaluation of safety and performance with and without ShieldNN.

and outputs a latent vector that encodes the state of the surroundings. The inputs to the PPO Network are: The latent vector $[z_1, \dots, z_{dim}]$, the vehicle's inertial measurements (current steering angle δ_f^c , speed v and acceleration a) and the relative angle ξ and distance r between the vehicle and the nearest obstacle. The latter two measurements are estimated using an obstacle detection module that takes the vehicle's LIDAR data as input. In our experiments, we assume we have a perfect obstacle detection estimator and we implement it by collecting the ground truth position and orientation measurements of the vehicle and the obstacles from CARLA then calculating ξ and r . The PPO network outputs the new control actions: Throttle ζ and steering angle δ_f . We omit using the brakes as part of the control input vector, as it is not necessary for this task. However, the RL agent will still be able to slow down the vehicle by setting the throttle value to 0 due to the simulated wheel friction force in CARLA. The throttle control action ζ gets passed directly to CARLA, while the steering angle control action gets filtered by ShieldNN. The filter also takes ξ and r as input and generates a new safe steering angle δ_f^s . To train the VAE, we first collect 10,000 images by driving the vehicle manually in CARLA along the desired route with obstacles spawned at random locations and observing different scenes from different orientations. We train the VAE encoder with cross validation and early-stopping. Then, after convergence, we check the output image to validate the VAE encoder.

ShieldNN Parameters: The ShieldNN filter is synthesized as in Section III with $\bar{r} = 4$ m, $\sigma = 0.48$ and KBM parameters $\delta_{f_{\max}} = \pi/4$, $l_f = l_r = 2m$, and $v_{\max} = 20m/s$.

A. Experiment 1: Safety Evaluation of ShieldNN

The goal of this experiment is to validate the safety guarantees provided by ShieldNN when applied to non-safe controllers. To do this, we evaluate the three trained agents in the same environment they were trained in, and with obstacles spawned randomly according to the same distribution used during training. With this setup, we consider two evaluation scenarios: (i) when the ShieldNN filter is in place (ShieldNN ON) and (ii) when ShieldNN filter is not in place (ShieldNN OFF). Table I shows all six configurations of this experiment. For each configuration, we run 200 episodes and record three metrics: (i) the minimum distance between the center of the vehicle and the obstacles, (ii) the average percentage of track completion, and (iii) the percentage of hitting obstacles across the 200 episodes.

Fig. 3a and 3b show the histograms of the minimum distance to obstacles for each configuration. The figure also show two vertical lines at 2.3 m and 4 m: the former is the minimum distance at which a collision can occur, given the length of the vehicle, and the latter is the value of the safe distance \bar{r} used to design the ShieldNN filter. Whenever the ShieldNN was not used in the 200 testing episodes (ShieldNN OFF, Fig. 3a), the average of all the

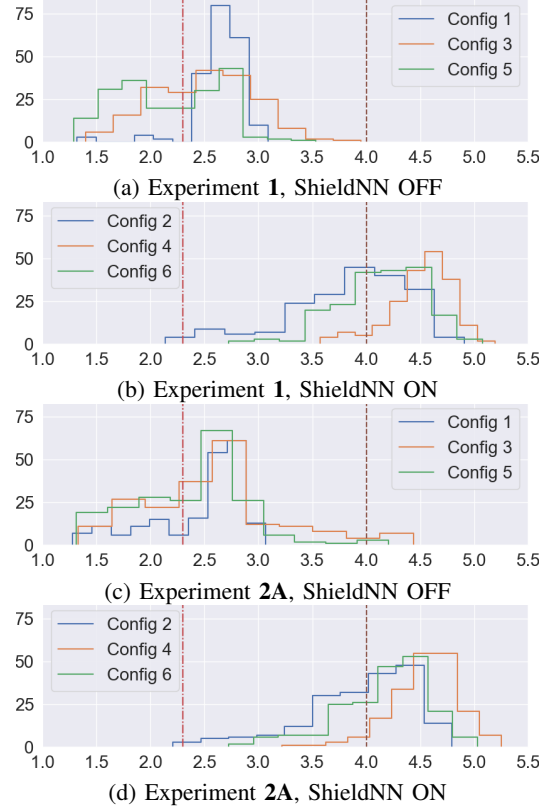


Fig. 3: Distributions of distance-to-obstacles for experiments 2 & 3, with and without ShieldNN.

histograms is close to the 2.3 m line indicating numerous obstacle collisions. The exact percentage of obstacle hit rate is reported in Table I. Upon comparing the histograms in Fig. 3a with those in 3b, we conclude that ShieldNN nevertheless renders all the three agents safe: note that the center of mass of the histograms shifts above the safety radius parameter, \bar{r} , used to design the ShieldNN filter. In particular, Agents 2 and 3 were able to avoid all the obstacles spawned in all 200 episodes, while Agent 1 hit only 0.5% of the obstacles spawned. Again, we believe this is due to the difference between the KBM used to design the filter and the actual dynamics of the vehicle. In general, the obstacle hitting rate is reduced by 99.4%, 100% and 100% for Agents 1, 2, and 3, respectively.

B. Experiment 2: Robustness of ShieldNN in Different Environments

The goal of this experiment is to test the robustness of ShieldNN inside a different environment than the training environment. We split the experiment into two parts:

Part 2-A: We use the same setup and metrics as in Experiment 1, but we perturb the locations of the spawned obstacles by a Gaussian distribution $\mathcal{N}(0, 1.5)m$ in the lateral and longitudinal directions. Fig. 3c and 3d show that despite this obstacle perturbation, ShieldNN is still able to maintain a safe distance between the vehicle and the obstacles whereas this is not the case when ShieldNN is OFF. Table I shows an overall increase of obstacle hit rate and a decrease in track completion rate when ShieldNN is OFF compared to the previous experiment. This is expected, as the PPO algorithm is trained with the obstacles spawned

at locations with a different distribution than the one used in testing. However, ShieldNN continues to demonstrate its performance and safety guarantees by having almost 100% track completion rate and almost 0% obstacle hit rate.

Part 2-B: This experiment is an evaluation of the ability (or not) of RL agents equipped with ShieldNN to generalize to novel environments. To evaluate performance in this setting, a transfer learning task is implemented where the pretrained Agents 2 and 3 are then *retrained* for 500 episodes in the new environment (compare to 6000 training episodes for the original experiments). The new environment is a city road surrounded by buildings, as opposed to the highway environment used for original training. This change substantially shifts the distribution of the camera input.

Fig. 4 shows the results for Configurations 4 and 6; recall from Table I in the main text that these configurations represent when (re)training is conducted with ShieldNN OFF and ON, respectively. Note that configuration 2 – where the original training was done in an environment with no obstacles – could not successfully complete the track during re-training for 500 episodes nor in testing, and is thus not included in the figure. Observe that in both configurations, the agent is still able to avoid obstacles for the 200 number of test episodes. Furthermore, configuration 6 (both retraining/testing with ShieldNN ON), the agent appears to behave more conservatively with respect to obstacle avoidance. ShieldNN still achieves the desired safety distance on average, and has exactly zero obstacle hits in both cases; it also has track completions of 98% and 97% respectively.

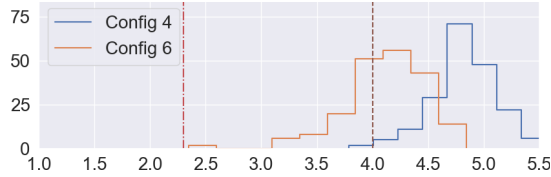


Fig. 4: Results of Experiment 3-B, distributions of metrics in a novel environment relative to training.

C. Experiment 3: Multiple Obstacles

In order to study the effectiveness of ShieldNN in providing safety in an environment where the vehicle can encounter multiple obstacles at the same time, we run 100 test scenarios in which we spawn multiple obstacles at random positions that are close to each other along the path of the vehicle. We compare between four variants based on a pretrained RL agent from Experiment 1 (Agent 2): 1) No filter, 2) SOSA filter; filtering PPO steering controls based on the closest obstacle to the vehicle. 3) MOSA; filtering PPO steering controls based on all detected obstacles. 4) MOSA plus penalizing the RL reward function with the unsafe action flag. This should disincentivize the RL agent from generating control actions that make the vehicle reach a state where MOSA cannot output a steering control action that is safe for all obstacles. We retrain the RL agent for 2000 episodes on scenarios that are different from the test scenarios. Then, we run the test scenarios with MOSA ON after retraining. As shown in Table II, using the naive approach (SOSA) reduces the obstacle hit rate significantly by 75% compared to the case when no filter is applied. Applying the proposed MOSA algorithm further reduces the obstacle hit rate by 36%. The trained RL agent with MOSA applied had the lowest obstacle hit rate of 4%. This shows that the RL agent is able to

	OHR%	TC%
No Filter	90	66
SOSA	22	73
MOSA (Before Retraining)	14	65
MOSA (After Retraining)	4	64

TABLE II: Experiment 3: Multiple Obstacles Scenarios. SOSA, single-obstacle safe action; MOSA, multiple-obstacle safe action; OHR, obstacle hit rate; TC, track completion

learn to avoid driving the vehicle into states where no safe action exists for all obstacles. Training the RL agent for more episodes does not improve obstacle hit rate results further. We notice that track completion percentage is relatively low for all test runs which is expected due to the fact that trying to avoid hitting multiple obstacles spawned randomly in the environment will cause the vehicle to move out of bounds of the track since ShieldNN only filters the steering control.

REFERENCES

- [1] A. D. Ames, S. Coogan, M. Egerstedt, G. Notomista, K. Sreenath, and P. Tabuada, “Control barrier functions: Theory and applications,” in *2019 18th European Control Conference (ECC)*. IEEE, 2019, pp. 3420–3431.
- [2] R. Cheng, G. Orosz, R. M. Murray, and J. W. Burdick, “End-to-end safe reinforcement learning through barrier functions for safety-critical continuous control tasks,” in *Proceedings of the AAAI Conference on Artificial Intelligence*, vol. 33, 2019, pp. 3387–3395.
- [3] L. Brunke, M. Greeff, A. W. Hall, Z. Yuan, S. Zhou, J. Panerati, and A. P. Schoellig, “Safe Learning in Robotics: From Learning-Based Control to Safe Reinforcement Learning,” *Annual Review of Control, Robotics, and Autonomous Systems*, vol. 5, no. 1, pp. 411–444, 2022. [Online]. Available: <https://www.annualreviews.org/doi/10.1146/annurev-control-042920-020211>
- [4] K.-C. Hsu, H. Hu, and J. F. Fisac, “The safety filter: A unified view of safety-critical control in autonomous systems,” *Annual Review of Control, Robotics, and Autonomous Systems*, vol. 7, 2023.
- [5] Z. Marvi and B. Kiumarsi, “Safe reinforcement learning: A control barrier function optimization approach,” *International Journal of Robust and Nonlinear Control*, vol. 31, no. 6, pp. 1923–1940, 2021.
- [6] M. H. Cohen and C. Belta, “Safe exploration in model-based reinforcement learning using control barrier functions,” *Automatica*, vol. 147, p. 110684, 2023.
- [7] J. Breeden and D. Panagou. (2023) Compositions of Multiple Control Barrier Functions Under Input Constraints. Comment: 9 pages, 7 figures, appearing in 2023 American Control Conference, extended version contains two additional remarks. [Online]. Available: <http://arxiv.org/abs/2210.01354>
- [8] M. Aali and J. Liu. (2022) Multiple Control Barrier Functions: An Application to Reactive Obstacle Avoidance for a Multi-steering Tractor-trailer System. [Online]. Available: <http://arxiv.org/abs/2209.05156>
- [9] J. Kong, M. Pfeiffer, G. Schildbach, and F. Borrelli, “Kinematic and dynamic vehicle models for autonomous driving control design,” in *2015 IEEE Intelligent Vehicles Symposium (IV)*. IEEE, 2015, pp. 1094–1099. [Online]. Available: <http://ieeexplore.ieee.org/document/7225830/>
- [10] S. Gu, L. Yang, Y. Du, G. Chen, F. Walter, J. Wang, and A. Knoll. (2024) A Review of Safe Reinforcement Learning: Methods, Theory and Applications. [Online]. Available: <http://arxiv.org/abs/2205.10330>
- [11] M. Alshiekh, R. Bloem, R. Ehlers, B. Könighofer, S. Niekum, and U. Topcu. (2017) Safe Reinforcement Learning via Shielding. [Online]. Available: <http://arxiv.org/abs/1708.08611>
- [12] X. Xu, P. Tabuada, J. W. Grizzle, and A. D. Ames, “Robustness of Control Barrier Functions for Safety Critical Control,” *IFAC-PapersOnLine*, vol. 48, no. 27, pp. 54–61, 2015. [Online]. Available: <http://arxiv.org/abs/1612.01554>
- [13] J. Ferlez, M. Elnaggar, Y. Shoukry, and C. Fleming, “ShieldNN: A provably safe NN filter for unsafe NN controllers,” 2024. [Online]. Available: <https://arxiv.org/abs/2006.09564>
- [14] A. Dosovitskiy, G. Ros, F. Codevilla, A. Lopez, and V. Koltun, “CARLA: An open urban driving simulator,” in *Proceedings of the 1st Annual Conference on Robot Learning*, 2017, pp. 1–16.
- [15] J. Schulman, F. Wolski, P. Dhariwal, A. Radford, and O. Klimov, “Proximal policy optimization algorithms,” *arXiv preprint arXiv:1707.06347*, 2017.
- [16] A. Raffin, A. Hill, K. R. Traoré, T. Lesort, N. Díaz-Rodríguez, and D. Filliat, “Decoupling feature extraction from policy learning: assessing benefits of state representation learning in goal based robotics,” *arXiv preprint arXiv:1901.08651*, 2019.

APPENDIX I DISCUSSION

Question 1: Why is ShieldNN is different from other CBFs? The main distinction between ShieldNN and other CBF approaches can be summarized succinctly: ShieldNN does not design a controller at all, much less a *single* safe controller. Rather, ShieldNN designs one NN component that can be used to enforce safety *on any* controller, no matter how that controller was designed. This architecture gives ShieldNN two unique capabilities: (i) ShieldNN can be immediately applied to a black-box controller; and (ii) ShieldNN can be employed *during* RL training of a controller, a situation where the (learned) controller is constantly changing. In particular, optimization-based approaches — that encode the CBF as a constraint in the numerical optimization problem — cannot directly be used for the setup in the experimental section where the controller processes data collected from cameras and LiDARs to train a neural network.

Question 2: Since ShieldNN is based on the simple KBM model, will ShieldNN still work for real-world scenarios? We address this concern in two ways.

1) Several empirical studies have evaluated the effectiveness of designing controllers for actual four-wheeled vehicles, using only the KBM as a model for their dynamics [9]. By means of experimental data collected from vehicles on a real-world test track, this reference showed evidence that the KBM is actually a viable approximation to real-vehicle dynamics with regard to controller design.

2) We validated our approach using CARLA, a simulator that simulates a much higher-fidelity dynamical model than the KBM. Even with direct parameter matching between the KBM and the CARLA vehicle, our simulation results show that ShieldNN was almost 100% effective at avoiding collisions.

Our results do not provide the same evidence of correctness for more complicated, non-KBM dynamical models. However, we view this as a problem for future work: having established a functioning ShieldNN filter for the KBM, we can in the future focus on bounding the errors between the KBM and more complicated dynamical models, thereby obtaining more general evidence of correctness (and with some hope of success, based on points 1 and 2 above).

Question 3: Are there any side effects of ShieldNN? In our experiments, applying ShieldNN during training had the side effect of creating a higher curb hitting rate during both training and testing, as compared to the case when the agent was trained with ShieldNN OFF. In particular, after training for 6000 episodes, the curb hitting rate for agent 2 went from 100% down to 8%. However for agent 3 it went from 100% down to 30%. This is due to the fact that ShieldNN forces the vehicle to steer away from facing an obstacle which, in turn, increases the probability of hitting one of the sides of the road. This side effect suggests the possibility for future research in generalizing ShieldNN to provide safety guarantees against hitting environment boundaries as well.

Question 4: Are there other current limitations of ShieldNN? In addition to the use of the KBM model, another potential limitation of ShieldNN is that it currently applies to single obstacles in a one-at-a-time fashion. We regard the extension to multiple obstacles to be a problem for future work and argue this is a problem for which the simple safe-control sets identified in ShieldNN will nevertheless

be useful. We aim to combine multiple ShieldNNs together in a compositional way to reason about multiple obstacles simultaneously.

APPENDIX II PROOFS FOR SECTION 4

There are two claims from Section IV that require proof.

- 1) First, we stated Theorem 1 without proof.
- 2) Second, we claimed that for any KBM parameters $\ell_r = \ell_f$ and $\delta_{f_{\max}}$, there exists a safety radius, \bar{r} , and a barrier parameter, σ , such that $h_{\bar{r},\sigma}$ and $\alpha_{v_{\max}}$ (as defined in (8) and (10)) comprise a barrier function for the KBM.

We provide proofs for each of these in the next two subsections after introducing some additional needed notation.

A. Additional Notation

Throughout the rest of this appendix we will use the following notation:

$$\begin{aligned} \mathcal{L}_{\bar{r},\sigma,\ell_r}(\chi, \beta) &\triangleq \nabla_{\chi}^T h_{\bar{r},\sigma}(\chi) \cdot f_{\text{KBM}}(\chi, (\beta, a)) \\ &= v \left(\frac{\sigma}{2 \cdot \bar{r} \cdot r} \sin(\xi/2) \sin(\xi - \beta) + \right. \\ &\quad \left. \frac{\sigma}{2 \cdot \bar{r} \cdot \ell_r} \sin(\xi/2) \sin(\beta) + \frac{\cos(\xi - \beta)}{r^2} \right). \end{aligned} \quad (25)$$

Where f_{KBM} is the right-hand side of the ODE in (3) and the variable a is merely a placeholder, since the (25) doesn't depend on it at all. In particular, (25) has the following relationship with (13):

$$\mathcal{L}_{\bar{r},\sigma,\ell_r}(\xi, \beta, v) = \mathcal{L}_{\bar{r},\sigma,\ell_r}((r_{\min}(\xi), \xi, v), \beta). \quad (26)$$

Moreover, we define the following set:

$$\tilde{\mathcal{C}}_{h_{\bar{r},\sigma}} \triangleq \{ \chi' = (r', \xi', v') \mid h(\chi') \geq 0 \wedge 0 < v' \leq v_{\max} \}, \quad (27)$$

which is the subset of the zero-level set of $h_{\bar{r},\sigma}$ that is compatible with our assumption that $0 < v \leq v_{\max}$ (see Problem 1).

B. Proof of Theorem 1

We prove the first claim of Theorem 1 as the following Lemma.

Lemma 1. Consider any fixed parameters \bar{r} , ℓ_r , σ and $v_{\max} > 0$. Furthermore, define

$$K_{\bar{r},\sigma} \triangleq \max(\{1, 1/\bar{r}\}) \cdot \left(\frac{\sigma}{2 \cdot \bar{r}} + 2 \right). \quad (28)$$

Now suppose that $h_{\bar{r},\sigma}$ is as in (8), and $\alpha_{v_{\max}}$ is as in (10) with K is chosen such that $K \geq K_{\bar{r},\sigma}$.

Then for each $(\xi, v, \beta) \in [-\pi, \pi] \times (0, v_{\max}] \times [-\beta_{\max}, \beta_{\max}]$, the function

$$L_{\xi,v,\beta} : r \in [\bar{r}, \infty) \mapsto \mathcal{L}_{\bar{r},\sigma,\ell_r}((r, \xi, v), \beta) + \alpha_{v_{\max}}(h_{\bar{r},\sigma}((r, \xi, v))) \quad (29)$$

is increasing on its domain, $\text{dom}(L_{\xi,v,\beta}) = [\bar{r}, +\infty)$.

Remark 2. Note the relationship between the function $L_{\xi,v,\beta}$ in (29) and the function used to define $R_{h,\alpha}$ in Corollary 1. That is the set that we are interested in characterizing in Theorem 1.

Proof. We will show that when $K \geq K_{\bar{r},\sigma}$, each such function $L_{\xi,v,\beta}$ has a strictly positive derivative on its domain. In particular, differentiating $L_{\xi,v,\beta}$ gives:

$$\begin{aligned} \frac{\partial}{\partial r} L_{\xi,v,\beta}(r) &= \frac{\partial}{\partial r} \left[\mathcal{L}_{\bar{r},\sigma,\ell_r}((r, \xi, v), \beta) + \alpha_{v_{\max}}(h_{\bar{r},\sigma}((r, \xi, v))) \right] \\ &= v \left(-\frac{\sigma}{2 \cdot \bar{r} \cdot r^2} \sin(\xi/2) \sin(\xi - \beta) - 2 \frac{\cos(\xi - \beta)}{r^3} \right) \\ &\quad + \frac{K \cdot v_{\max}}{r^2} \\ &\geq v \left(-\frac{\sigma}{2 \cdot \bar{r} \cdot r^2} - \frac{2}{r^3} \right) + \frac{K \cdot v_{\max}}{r^2}. \end{aligned} \quad (30)$$

To ensure that this derivative is strictly positive, it suffices to choose K such that

$$v \left(-\frac{\sigma}{2 \cdot \bar{r} \cdot r^2} - \frac{2}{r^3} \right) + \frac{K \cdot v_{\max}}{r^2} \geq 0. \quad (31)$$

For this, we consider two cases: $\bar{r} < 1$ and $\bar{r} \geq 1$.

When $\bar{r} \geq 1$, then $1/r^3 \leq 1/r^2$ for all $r \geq \bar{r}$. Thus it suffices to choose K such that

$$K \geq \frac{v}{v_{\max}} \left(\frac{\sigma}{2 \cdot \bar{r}} + 2 \right), \quad (32)$$

which is assured under the assumption that $v \in (, v_{\max}]$ if

$$K \geq \frac{\sigma}{2 \cdot \bar{r}} + 2. \quad (33)$$

Now, when $\bar{r} < 1$, choosing K according to (33) ensures that (31) is true for all $r \geq 1$. Thus, we also have to ensure (31) holds for $\bar{r} \leq r < 1$. But in this case, $1/r^3 \geq 1/r^2$, so (31) will be satisfied if

$$K \geq \frac{1}{\bar{r}} \left(\frac{\sigma}{2 \cdot \bar{r}} + 2 \right). \quad (34)$$

Thus, the desired conclusion holds if we choose $K \geq K_{\bar{r},\sigma}$ as defined in the statement of the lemma. \square

Now, we have the prerequisites to prove Theorem 1.

Proof. (Theorem 1) The first claim of Theorem 1 is proved as Lemma 1. Thus, it remains to show that for any $\chi = (r, \xi, v) \in \mathcal{C}_{h_{\bar{r},\sigma}}$ with $v \in (0, v_{\max}]$ — that is $\chi \in \tilde{\mathcal{C}}_{h_{\bar{r},\sigma}}$ — we have that (12) holds. However, this follows from Lemma 1.

In particular, choose an arbitrary $\chi' = (r', \xi', v') \in \tilde{\mathcal{C}}_{h_{\bar{r},\sigma}}$, and choose an arbitrary $\omega' = (\beta', a') \in R_{h_{\bar{r},\sigma}}((r_{\min}(\xi'), \xi', v'))$; as usual we will only need to concern ourselves with the steering control, β' . First, observe that by definition:

$$\begin{aligned} (\beta', a') &\in R_{h_{\bar{r},\sigma}}((r_{\min}(\xi'), \xi', v')) \\ \implies \mathcal{L}_{\bar{r},\sigma,\ell_r}((r_{\min}(\xi'), \xi', v'), \beta') + \\ &\quad \alpha_{v_{\max}}(h_{\bar{r},\sigma}((r_{\min}(\xi'), \xi', v'))) \geq 0. \end{aligned} \quad (35)$$

However, the conclusion of this implication can be rewritten using the definition (29):

$$(\beta', a') \in R_{h_{\bar{r},\sigma}}((r_{\min}(\xi'), \xi', v')) \implies L_{\xi',v',\beta'}(r_{\min}(\xi')) \geq 0. \quad (36)$$

We now invoke Lemma 1: since $r_{\min}(\xi') \geq \bar{r}$ by construction, Lemma 1 indicates that $L_{\xi',v',\beta'}$ is strictly increasing on the interval $[r_{\min}(\xi'), r']$. Combining this conclusion with (36), we see that $L_{\xi',v',\beta'}(r') \geq 0$. Again using the definition of $L_{\xi',v',\beta'}$ in (36), we conclude that

$$\mathcal{L}_{\bar{r},\sigma,\ell_r}((r', \xi', v'), \beta') + \alpha_{v_{\max}}(h_{\bar{r},\sigma}(r', \xi', v')) \geq 0. \quad (37)$$

Thus, we conclude that $(\beta', a') \in R_{h_{\bar{r},\sigma}}(\chi')$ by the definition thereof (see the statement of Theorem 1). Finally, since χ' and ω' were chosen arbitrarily, we get the desired conclusion. \square

C. Proof of That a Barrier Function Exists for Each KBM Instance

For $h_{\bar{r},\sigma}$ and $\alpha_{v_{\max}}$ to be a useful class of barrier functions, it should be that case that at least one of these candidates is in fact a barrier function for each instance of the KBM. We make this claim in the form of the following Theorem.

Theorem 2. Consider any KBM robot with length parameters $\ell_r = \ell_f$; maximum steering angle $\delta_{f_{\max}}$; and maximum velocity $v_{\max} > 0$. Furthermore, suppose that the following two conditions hold:

- 1) $\beta_{\max} \leq \pi/2$, or equivalently, $\delta_{f_{\max}} \leq \frac{\pi}{2}$;
- 2) $\frac{1}{\ell_r} (\sigma(1 - \sigma)\ell_r + \sigma\bar{r}) \sin(\frac{\pi}{4} + \frac{\beta_{\max}}{2}) \sin(\beta_{\max}) \geq 2$; and

Then for every $\chi = (r, \xi, v)$ such that $0 < v \leq v_{\max}$ the set $R_{h_{\bar{r},\sigma}}(\chi)$ is non-empty. In particular, the feedback controller (interpreted as a function of ξ only):

$$\pi : \xi \mapsto \begin{cases} -\beta_{\max} & \xi < -\epsilon \\ \xi & \xi \in [-\beta_{\max}, \beta_{\max}] \\ \beta_{\max} & \xi > \epsilon \end{cases} \quad (38)$$

is safe.

Remark 3. Note that there is always a choice of \bar{r} and $\sigma \in (0, 1)$ such that condition (ii) can be satisfied. In particular, it suffices for \bar{r} and σ to be chosen such that:

$$2 \frac{(\ell_r/\bar{r})}{\sin(\beta_{\max}) \sin(\pi/4 + \beta_{\max}/2)} \leq \sigma. \quad (39)$$

Thus, by making \bar{r} large enough relative ℓ_r , it is possible to choose a $\sigma \in (0, 1)$ such that the inequality (39) holds, and (ii) is satisfied.

Proof. (Theorem 2) As a consequence of Theorem 1, it is enough to show that $R_{h_{\bar{r},\sigma}}((r_{\min}(\xi), \xi, v_{\max}))$ is non-empty for every $\xi \in [-\pi, \pi]$.

The strategy of the proof will be to consider the control $\beta = \pi(\xi)$, and verify that for each $\chi = (r, \xi, v) \in \tilde{\mathcal{C}}_{h_{\bar{r},\sigma}}$ such that $\xi \in [0, \pi]$, we have:

$$\mathcal{L}_{\bar{r},\sigma,\ell_r}(\xi, \pi(\xi)) \geq 0. \quad (40)$$

The symmetry of the problem will allow us to make a similar conclusion for $\xi \in [-\pi, 0]$.

We proceed by partitioning the interval $[0, \pi]$ into the following three intervals:

$$I_1 \triangleq [0, \beta_{\max}], \quad I_2 \triangleq (\beta_{\max}, \pi/2 + \beta_{\max}], \quad I_3 \triangleq (\pi/2 + \beta_{\max}, \pi].$$

and consider the cases that ξ is in each such interval separately.

Case 1 $\xi \in I_1$: In this case, $\pi(\xi) = \xi$, and $\xi \leq \beta_{\max} \leq \pi/2$ by assumption. It is direct to show that:

$$\cos(\xi - \pi(\xi)) = \cos(0) \geq 0 \quad (41)$$

and

$$\sin(\xi/2) \sin(\xi - \pi(\xi)) = 0. \quad (42)$$

Hence, the \cos term in (13) can be lower bounded by zero, and the first term in (13) is identically zero by (42). Thus, in this case, (13) is lower bounded as as:

$$\mathcal{L}_{\bar{r}, \sigma, \ell_r}(\xi, \beta_{\max}) \geq \frac{\sigma \cdot v \cdot \sin(\xi/2) \sin(\pi(\xi))}{2 \cdot \bar{r} \cdot \ell_r}, \quad (43)$$

which of course will be greater than zero since $\xi \in I_1 = [0, \beta_{\max}]$ with $\beta_{\max} \leq \pi/2$ by assumption (i).

Case 2 $\xi \in I_2$: In this case, $\pi(\xi) = \beta_{\max}$. Thus, for $\xi \in I_2$, we have that:

$$\cos(\xi - \beta_{\max}) \geq 0 \quad (44)$$

$$\sin(\xi/2) \sin(\xi - \beta_{\max}) \geq 0 \quad (45)$$

$$\sin(\xi/2) \sin(\beta_{\max}) \geq 0. \quad (46)$$

Consequently, (40) is automatically satisfied, since all of the quantities in the Lie derivative are positive.

Case 3 $\xi \in I_3$: In this case, $\pi(\xi) = \beta_{\max}$ as in Case 2. However, the \cos term is now negative in this case:

$$0 > \cos(\xi - \beta_{\max}) \geq -\frac{1}{\bar{r}^2}. \quad (47)$$

Thus, since the other two terms are positive on this interval, we need to have:

$$\sin\left(\frac{1}{2}\left(\frac{\pi}{2} + \beta_{\max}\right)\right) \left(\frac{\sigma(1-\sigma)}{2 \cdot \bar{r}^2} \sin(\pi - \beta) + \frac{\sigma}{2 \cdot \bar{r} \cdot \ell_r} \sin(\beta) \right) \geq \frac{1}{\bar{r}^2}. \quad (48)$$

This follows because on I_3 , $\sin(\frac{\xi}{2}) \geq \sin(\frac{1}{2}(\frac{\pi}{2} + \beta_{\max}))$ and $\sin(\xi - \beta_{\max}) \geq \sin(\pi - \beta_{\max})$; i.e. we substituted the lower and upper end points of I_3 , respectively. Noting that $\sin(\pi - \beta_{\max}) = \sin(\beta_{\max})$, we finally obtain:

$$\sin\left(\frac{1}{2}\left(\frac{\pi}{2} + \beta_{\max}\right)\right) \sin(\beta_{\max}) \left(\frac{\sigma(1-\sigma)}{2} + \frac{\sigma \bar{r}}{2 \cdot \ell_r} \right) \geq 1. \quad (49)$$

The preceding is just another form of (ii) so we have the desired conclusion in (40).

The conclusion of the theorem then follows from the combined consideration of Cases 1-3 and Theorem 1 as claimed above. \square